Analyzing Internal Resistance in Lithium Nickel Cobalt Oxide (LiNiCoO) Vehicle Batteries for Enhanced SOC and SOH Prediction

Tara Joshi
Department of Electrical and Computer Engineering
Kennesaw State University
Marietta, GA, US
tjoshi2@students.kennesaw.edu

Charlie Leon
Department of Electrical and Computer Engineering
Kennesaw State University
Marietta, GA, US
cleon4@students.kennesaw.edu

Mason Snyder
Department of Electrical and Computer Engineering
Kennesaw State University
Marietta, GA, US
msnyde43@students.kennesaw.edu

Anish Sankuratri
Department of Mechanical Engineering
Kennesaw State University
Marietta, GA, US
asankura@students.kennesaw.edu

Mustafa Raza
Department of Electrical and Computer Engineering
Kennesaw State University
Marietta, GA, US
mraza2@students.kennesaw.edu

Beibei Jiang*
Department of Electrical and Computer Engineering
Kennesaw State University
Marietta, GA, US
bjiang1@kennesaw.edu

Abstract*— Internal resistance of a battery reflects its distinct characteristics, including factors such as state of health (SOH), state of charge (SOC), reversibility, thermal runaway, etc. Variation of the internal resistance with the testing currents (i.e. C-rate) suggests a relationship between internal resistance and the number of charges stored in the electrode materials (i.e. the SOC of the battery). Additionally, internal resistance is influenced by the homogeneity of the charge distribution under various testing currents (i.e. whether the charges are locally distributed near the surface area due to diffusion limitations or homogeneously stored in the electrode materials). The determination of internal resistance and the examination of the correlation between internal resistance and deliverable capacity can be utilized to predict the SOH and SOC of the battery, and even to understand its aging mechanisms. The paper introduces a simple approach based on modified intermittent current interruption (ICI) methods to characterize the internal resistance at controlled voltage (or SOC). The paper elucidates that the lifetime of a battery can be divided into four stages - initial stages, transition states, stable states, and aged stages, wherein each stage exhibits a unique relationship between internal resistance and SOC. The stable stage of the battery is characterized by the lowest internal resistance among the four stages. Both the stable stages and transition stages exhibit a distinctive decreasing trend in internal resistance while increasing SOC. The paper also identifies a robust correlation between the usable capacity of the battery and internal resistance, in which the deliverable capacity experiences a significant drop when internal resistance increases, particularly in aged batteries and batteries tested under large testing current. An analytical model is proposed to correlate the rise in internal resistance with changes in deliverable capacity, SOC, and SOH under various testing currents. Furthermore, when integrated with the Electrochemical Impedance Spectroscopy (EIS) methods, the correlation of internal resistance becomes a valuable tool for predicting SOC and SOH and comprehending the battery's aging mechanisms.

Keywords—internal resistance, vehicle battery, state-of-health, state-of-charge, Battery Management System (BMS)

This work was funded by FYSP and URCA program of Kennesaw State University.

I. INTRODUCTION

Lithium-ion batteries (LIBs), as the most versatile and attractive energy storage systems, have fueled the global scale adoption of numerous portable electronics which rapidly became integral to daily life during the past 30 years. [1] In addition, their pivotal role in the advancement of electric vehicles (EVs) and renewable energy technologies positions LIBs as key players in the global pursuit of zero-carbon emissions and propel us towards a cleaner and greener future. With the growing prevalence of EVs powered by LIBs, ensuring the reliability and safety of these vehicle batteries has become an urgent priority. The Battery Management System (BMS) is an essential component in EVs to ensure reliable operations of each battery. Employing measurable factors like voltage, current, temperature, and more, BMS can predict and monitor the critical parameters of battery, including the state of charge (SOC) and state of health (SOH).[2] SOC, which indicates the internal charge level of the batteries, reflects the usable capacity of the batteries. [3] The accurate SOC is needed in predicting the remaining mileage of an EV. Besides, the accurate determination of SOC is required to avoid safety issues, such as overcharge, deep discharge, thermal runaway or even explosion. [4] On the other hand, SOH, which is defined as the ratio between usable capacity and the initial capacity of the fresh call, is a useful indicator for accessing the ageing conditions of the battery. [3] The accurate determination of SOH is essential for optimizing performance, predicting mileage range, ensuring safety, and managing costs of EVs.

The ongoing investigations into SOC estimation can be classified into three primary categories. The Coulomb Counting Method (CCM) is based on the definition of SOC, obtained by the ratio of integrating current with time, to the theoretical capacity. However, the accuracy of CCM estimation is largely limited by the challenge of unknown initial SOC values. [4, 5] The Open Circuit Voltage (OCV) method is also widely employed for SOC estimation, as the electrochemical potential is closely related to the active

SoutheastCon 2024 | 979-8-3503-1710-7/24/$31.00 ©2024 IEEE | DOI: 10.1109/SOUTHEASTCON52093.2024.10500138

charges remaining in the electrodes. [6, 7] Data mapping, describing the SOC-OCV relationships, is typically derived from the lookup tables obtained through long-term laboratory tests. However, the OCV method necessitates a long relaxation time (>2h) for the battery to reach equilibrium for accurate OCV measurement, restricting its practical application.[4] The third method includes various algorithms based on equivalent circuit models (ECM) designed as observers/filters. These algorithms use current and voltage measurements with feedback corrections to offer precise SOC estimations. However, their efficacy relies heavily on the accuracy and complexity of the employed model. [4, 8] Therefore, there is an urgent need to explore alternative methods for accurate and efficient SOC estimation to construct an efficient BMS for EVs.

Internal resistance is a vital battery parameter, and when coupled with OCV data, it becomes a valuable tool for predicting both the SOC and SOH of the battery. [6] The observed correlation between increased internal resistance and the loss of capacity as cycle number increases highlights the significance of internal resistance as a pivotal indicator of the SOH of battery. [9] Variation of the internal resistance with the testing currents (i.e. C-rate) suggests a relationship between internal resistance and the number of charges stored in the electrode materials (i.e. the SOC of the battery). Additionally, internal resistance is influenced by the homogeneity of the charge distribution under various testing currents (*i.e.* whether the charges are locally distributed near the surface area due to diffusion limitations or homogeneously stored in the electrode materials). The combination of galvanostatic cycling and a modified intermittent current interruption (ICI) method offers a rapid, accurate and comparatively simple analytical approach for determining internal resistance and tracking changes in internal resistance over long time cycling.

A generalized ECM, as depicted in **Fig. 1**, is commonly employed to simulate both the transient and steady response of the battery when determining the internal resistance. The ECM comprises an ohmic resistance (R_b), a parallel RC network, a DC source (V_{oc}) representing the OCV of the battery, and V(t) representing the measured terminal voltage. Since the capacitor normally acts as an open circuit in the case of DC circuit, using Kirchhoff's law, V(t) can be expressed as:

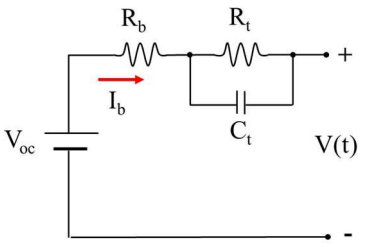

Fig. 1. A generalized ECM for batteries.

Charging

Discharging

where is internal resistance, and

.

When current is interrupted and turned off in the ICI method, an instantaneous transient voltage variation (ΔV) occurs. Consequently, the value can be calculated using the fundamental ohmic law (i.e. =ΔV/I), as illustrated in Fig. 2. This approach can be executed using a conventional battery tester or even with standard battery charging systems, which are implementable for real-time use and can be transferred to BSM. [10, 11] However, is notably influenced by the sampling frequency, *i.e.*, the time (t) after current is interrupted, due to distinct time constants associated with different electrochemical processes. At short sampling time (such as t≤2ms), the instantaneous voltage drop ΔV is attributed to pure ionic resistance of the bulk electrolyte, which typically remains unchanged with the SOC of the battery. [10] With time passing (*i.e.* t=1s), charge transfer reactions will contribute to the instantaneous voltage drop ΔV, causing the value to exhibit dependence on both the SOC and SOH of the battery. [10] If the sampling frequency is too large (*i.e.* t>>1s), the measured will incorporate the contribution due to the diffusion process, which adds the complexity of the analysis. Therefore, the choice of sampling time requires a delicate balance between data accuracy and the convenience of data sampling.

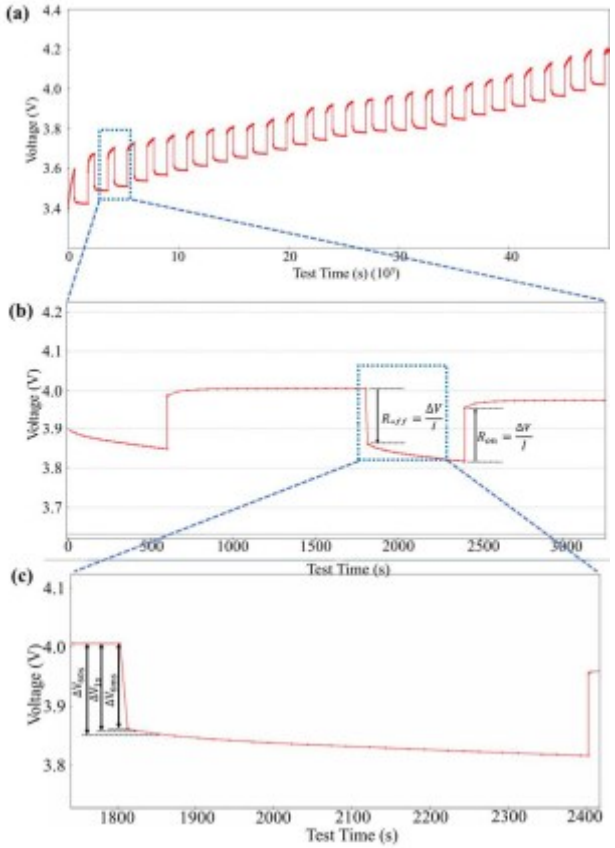

Fig. 2. (a) Example of the ICI implementation during charge step; (b) The voltage response after the current is interrupted. ΔV can be used to calculate the value of internal resistance; (c). Voltage response at different sampling time (*i.e.* t=6ms, 1s, 60s) after current interruption.

II. Method Description

A. Exploring with SOC via Modified ICI method A.

All experiments were conducted on commercially available Lithium Nickel Cobalt Oxide ($LiNi_xCo_{1-x}O_2$) coin cell batteries manufactured by Cornell Dubilier (CR3032, 200mAh, nominal voltage is 3.7V, voltage window is 3-4.2V). To activate the fresh batteries and form stable solid-electrolyte-interface (SEI) layer, all the fresh batteries were galvanostatically cycled at 0.1C (20mA) in the voltage window of 3.0-4.2V (Arbin battery testing system, LBT21084) at room temperature for 4-5 cycles. The modified ICI method A, as depicted in **Fig. 2 (a)**, was employed to monitor the correlation between and SOC under various

current rates. In this method, a short current pulse of low current (*i.e.* 0.1C to 0.4C) was applied to charge or discharge the battery, inducing a 5% to 10% change in the battery's SOC. Subsequently, the current was interrupted and turned off during the following rest step, allowing the battery to relax for 20 minutes before the next current pulse. The rest interval was intended to monitor the at specific SOC as well as to enable the battery to reach equilibrium or quasi-equilibrium.

As depicted in **Fig. 2(b)**, after the current is interrupted during charging, the voltage drops instantaneously during the first few seconds, and then decreases with a linear relationship with the square root of the time due to the diffusion process. The internal resistance measured after current is turned off at specific sampling time (*i.e.* R_{off}) will be used to simulate .
In addition, as depicted in **Fig. 2 (c)**, ΔV is dependent on the choice of sampling time (t). In this study, ΔV at three different sampling time (*i.e.* ΔV_{6ms}, ΔV_{1s}, ΔV_{60s}) were analyzed to simulate the true .

B. Exploring with usable capacity via Modified ICI method B.

To identify the correlation between with the usable capacity and the SOH, the batteries were galvanostatically cycled at 0.1C-0.5C for 500 cycles. A new modified ICI method was implemented by inserting a rest step after each full charge and discharge step. The ΔV_{1s} was utilized to calculate the internal resistance after charge (*i.e.* $R_{int\text{-}charge}$) and the internal resistance after discharge (*i.e.* $R_{int\text{-}discharge}$).

C. Electrochemical impedance spectroscopy (EIS) method.

Electrochemical impedance spectroscopy (EIS) was performed on each battery after the battery is fully discharged or charged with a Gamry Interface 1010E Potentiostatic at room temperature. The EIS test was measured at AC voltage of 10mV in the frequency range of 10mHz to 1MHz with 10 points/decade. The EIS spectrum was analyzed using Z-viewer software, employing Randle's equivalent circuit model to monitor changes within the battery and gain insights into the aging mechanism.

III. Results and Discussion

A. The charging-discharging profile

The galvanostatic charge and discharge curves for the first four cycles tested at 0.1C (20mA) were displayed in **Fig.3**. The SOC values were calculated based on a theoretical capacity of 200mAh after charging to 4.2V and were displayed on the right Y-axis. Notably, rapid voltage changes (~25% of the overall voltage change in the window of 3-4.2V) occurred at the beginning of the charging curves and at the end of the discharging curves, while contributing to small SOC change (<5%). A short voltage plateau at 3.7-3.8V was evident on both curves. Across other regions on the charge and discharge curves, a near linear relationship between voltage and capacity was observed.

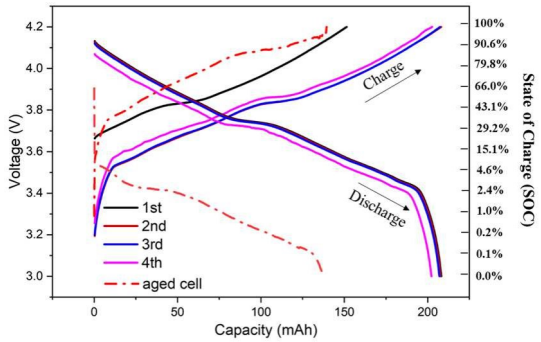

Fig.3. The charging and discharging profile of the fresh cell and aged cell tested at 0.1C (20mA).

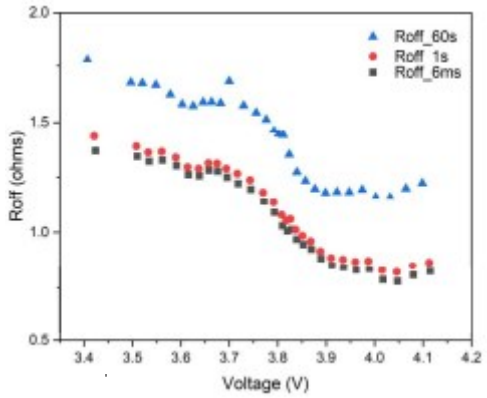

Fig. 4 The R recorded during the charging step at different sampling time of t=6ms, 1s, 60s.

The plot also includes the galvanostatic curve for the aged cell, revealing a reduced deliverable capacity of 139mAh, which is 70% of the initial theoretical value. Furthermore, the voltage exhibited an immediate jump from the OCV of 3.28V to 3.56V upon charging and a swift drop from OCV of 3.90V to 3.55V upon discharging. This huge change in voltage suggests a significant increase in R for the aged cell.

B. The correlation between and SOC

The modified ICI method (as described in Fig. 2) was used to monitor the while varying the SOC during the charging and discharge steps. **Fig. 4** depicts the obtained

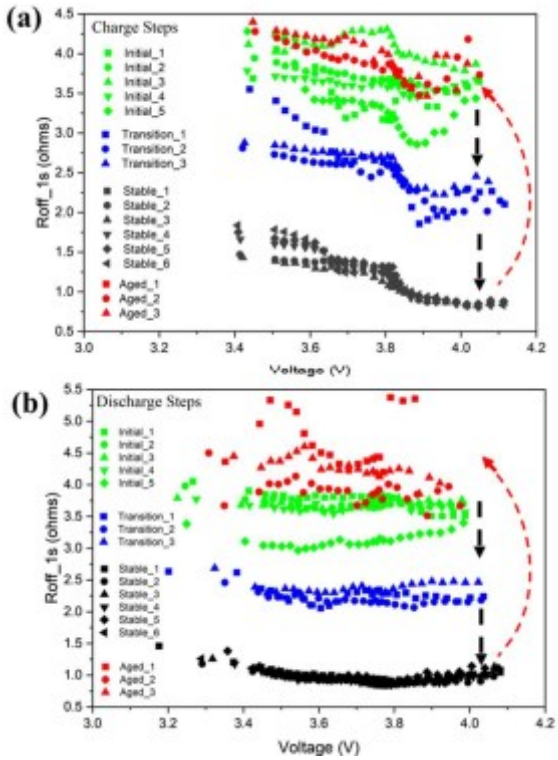

Fig. 5. The dependence of internal resistance with voltage during (a) charging and (b) discharge steps.

at different sampling time (t) during the charge step. The three curves exhibit a similar decreasing trend as SOC increases, with gradually decreasing at the initial phase of charging, experiencing a significant decreasing near the voltage plateau voltage of 3.8V, followed by a gradual decrease until fully charged. The values of at 1 second (s) and 6 ms are close, while at 60 s is higher. This discrepancy arises because, at t=60 s, the diffusion process contributes to additional voltage changes, whereas at 1s and 6ms, the voltage changes are primarily driven by charge transfer. It is noteworthy that t=1s represents the most practical sampling frequency for most battery testers, and the reported R_{off} was calculated at sampling time of t=1s to simulate the true R.

The correlation between and SOC during various life stages of a battery were analyzed to provide a comprehensive understanding of the . The plots presented in **Fig. 5**(a) depict the representative charging steps throughout the battery's entire lifespan. The lifetime of the battery can be divided into four stages, each characterized by a distinct relationship between and SOC. These stages are initial stages, transition states, stable states, and aged stages.

The curves for the initial stages occupy the top positions of the graph and span relatively wide ranges from 3.0-4.5 ohms. As the battery approaches the transition stages, the curves gradually drop to lower values. After transitioning, the battery enters the stable states, where the significantly drops to the lowest values. In the last aging states, the curves jump back to reach or surpass the high values of the unactivated initial states, owing largely to degradation mechanisms such as the consumption of liquid electrolyte, the formation of thicker SEI layer, and damage to electrode structure. [12, 13]. It is worth noting that the correlation between and Voltage/SOC exhibits a characteristic pattern for both the transition and stable states, where gradually decreases as Voltage and SOC increases, with a significant change in near the voltage plateau at 3.8V. The for the fully charged state (*i.e.* SOC=100%) is lower than that at the fully discharged state (*i.e.* SOC=0%).

As depicted in **Fig. 5** (b), comparable conclusions are evident in the discharge cycles, revealing the distinguishable four stages. The stable stages exhibit the lowest during the discharge cycles as well. In the final states of the battery's life, aging induces a jump in the internal resistance curves, surpassing the values of the initial cells, indicating notable degradations to the electrode micro- and macro-structures and/or poor interfacial contacts. Consequently, the correlation

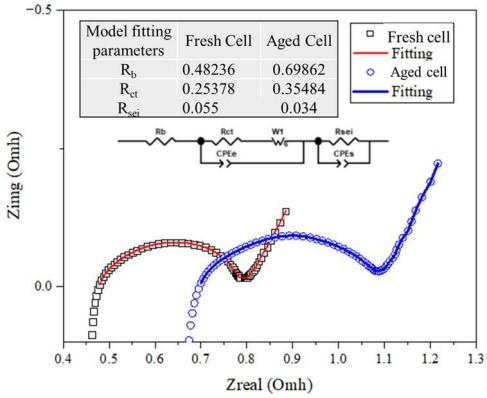

Fig.6. The Nyquist plots of the EIS tests for fresh cell and the aged cell. The two plots were fitted by the equivalent circuit model (ECM), and the fitting results were shown as insets of this figure.

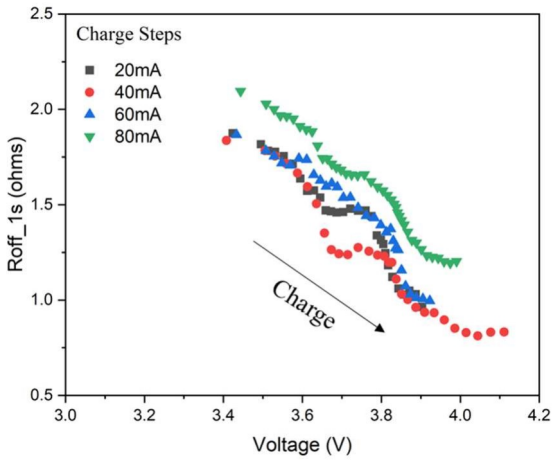

Fig.7. The dependence of with voltage during the charge steps tested at different currents of 20mA, 40mA, 60mA, and 80mA.

between the increased accompanied by the loss of capacity strongly indicates the aging and degradation of the battery.

C. *Electrochemical Impedance Spectroscopy (EIS)*

The EIS spectrum can distinguish different resistance mechanisms, thus influencing the interpretation of overall impedance/resistances. [14] **Fig. 6** shows the Nyquist plot of EIS spectrum for both the fresh cell and the aged cell. The EIS spectrum was fitted using the Randels' ECM depicted in the inset of the figure, and the fitting results were also presented in the figure. The intercept of the EIS spectrum reflects the total bulk resistance of the electrolyte, separator, and electrodes (denoted as). The first semicircle typically originates from the impedance of the solid electrolyte interphase (SEI) layer (denoted as).[14] When the SEI layer forms due to the decomposition of electrolyte on the anode materials, it consumes extra lithium ions, thus leading to a capacity reduction as well as increase in R. [15, 16] The second semicircle is related to charge transfer resistance of the lithiation/delithiation process (denoted as !). R" reflects the kinetics of an electrochemical reaction, it is therefore a useful indicator for understanding the electrode reaction processes. [14]. The value increases significantly from 0.48236 ohms to 0.69862 ohms for the aged cell,

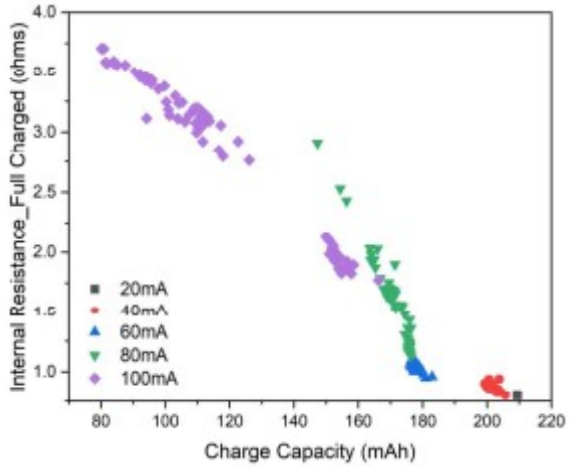

Figure 8. The internal resistance of the fully charged battery and the deliverable capacity tested at different currents of 20mA, 40mA, 60mA, 80mA, and 100mA.

indicating large consumption of the liquid electrolyte. Meanwhile, ! for the aged cell increases as well, which can be attributed to the irreversible structural damages to the electrode materials. [17, 18]

The EIS results confirmed the increased resistance for the aged cell arise from two distinct mechanisms: , unaffected by test currents and SOC, and !, influenced by both test currents and SOC. Consequently, the obtained by the ICI methods is shaped by these two mechanisms. The correlation between and SOC can be ascribed to the characteristics of the component of the !.

D. Dependence of Internal Resistance with test currents

Fig. 7(a) shows the dependence of with voltage at various testing currents during the charging step. The tested at higher current (*i.e.* 80mA) exhibits a similar decreasing trend as voltage increases, with the curves shifting upwards at high testing currents, indicating elevated at higher testing currents. Meanwhile, the galvanostatic charge and discharge tests at higher testing current of 80mA reveal a reduced capacity of 175mAh, which is 87.5% of the theoretical capacity. This reconfirms the correlation between increased internal resistance with the loss of capacity when high testing current is applied to unaged cells.

E. Dependence of Internal Resistance with usable capacity

Given that is influenced by SOC and voltage, and it exhibits path-dependent characteristics, there is practical significance in monitoring the after complete charge and discharge of the battery by the employed modified ICI method (method B). Batteries underwent galvanostatic charging and discharging at various current densities, ranging from 20mA to 100mA, with interruptions occuring after the battery reached full charged and full discharged states to monitor the and the usable capacity.

Fig. 8 depicts the relationship between of the fully charged battery and its deliverable capacity. A robust correlation emerges between the usable cpacity of the battery and the . As increases, the deliverable capacity experiences a significant drop. This conclusion aligns consistently with the earlier observations. The correlation between the increase in and the loss in capacity can be attributed to battery aging, involving permannent changes in the battery structure. The correlation can also be linked to high testing current, which are more likely to accelerate battery aging compared to lower testing currents.

F. Mechanistic model

To elucidate the observed correlations between increased with the loss of capacity, a mechanistic model based on the charge-transfer process within the active cathode material is proposed. As depicted in **Fig. 9**, the representative model depicts the charge-transfer process (*i.e.* the delithiation process) of the Lithium Nickel Cobalt Oxide (#$%$&'()*&+,) during the charging step. Throughout the ongoing charging process, Li ions were gradually extracted out of the cathode materials, which leads to the gradual decreases in internal resistance of the battery. It is noteworthy that the charge transfer process prefers to occur in the surface layer of the active cathode material due to its shorter diffusion distance.

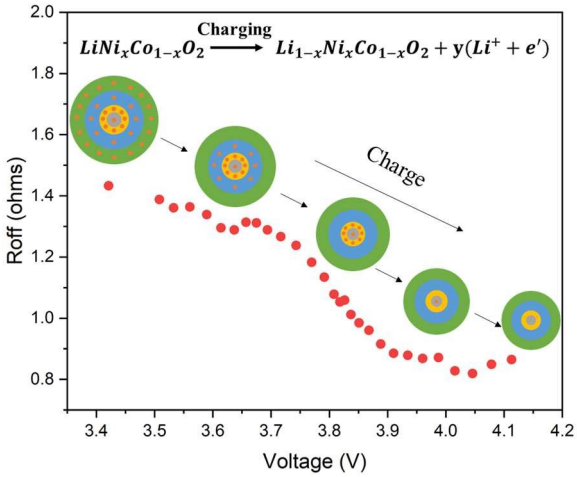

Fig. 9. The proposed model for explaining the observed correlation and the dependence on current density.

Under conditions providing ample time for ion diffusion process, as observed in conditions involving low to moderate currents, Li ions in the inner core of the active cathode material undergo complete extraction from the cathode materials upon charging, leading to a state with low . However, at elevated charging currents, where diffusion is limited, only the Li ions in the outer surface layers of active cathode material will be extracted until the charging cut-off voltage is reached. Meanwhile, Li ions in the inner core of active cathode materials remain in the material due to diffusion limitations. The greater the quantity of remaining Li ions in the inner core at high testing currents, the higher the internal resistance and the lower the delivered capacity.

IV. Conclusion

The work demonstrated the application of the modified ICI methods for characterizing the internal resistance and analyzing the correlation of internal resistance with SOC and voltage under different testing currents. The identification of four stages throughout the lifespan of the battery, wherein each stage exhibits a distinct relationship between internal resistance and SOC, coupled with the observation of a distinct decreasing trend in internal resistance while increasing SOC, positions internal resistance as a robust indicator for predicting the SOC of the battery. Meanwhile, the increased internal resistance accompanied by the loss of capacity indicates that internal resistance can be used to access the SOH of the battery. In addition, the EIS methods provide a strong validation for the trend observed while also providing some mechanistic understanding for correlating the change in internal resistance with different electrochemical processes. Finally, a mechanistic analytical model was proposed to correlate the increased internal resistance with the loss of capacity at elevated testing currents. All the conclusions affirm that that the internal resistance is a crucial parameter within the battery, capable of reflecting both the SOC and SOH of the battery. Additionally, the modified ICI methods for predicting internal resistance are simple and compatible with the BMS system.

Acknowledgment

We gratefully acknowledge the funding support from the First-Year Scholars Program from the Office of Undergraduate research at Kennesaw State University.

REFERENCES

[1] D. Di Lecce, R. Verrelli, and J. J. G. C. Hassoun, "Lithium-ion batteries for sustainable energy storage: recent advances towards new cell configurations," vol. 19, no. 15, pp. 3442-3467, 2017.

[2] M.-K. Tran *et al.*, "A comprehensive equivalent circuit model for lithium-ion batteries, incorporating the effects of state of health, state of charge, and temperature on model parameters," *Journal of Energy Storage,* vol. 43, p. 103252, 2021.

[3] J. F. Pakpahan, B. R. Dewangga, G. N. Pratama, A. I. Cahyadi, S. Herdjunanto, and O. Wahyunggoro, "State of charge estimation for lithium polymer battery using kalman filter under varying internal resistance," in *2019 International Conference on Information and Communications Technology (ICOIACT)*, 2019, pp. 839-844: IEEE.

[4] L. Sun, G. Li, F. J. R. You, and S. E. Reviews, "Combined internal resistance and state-of-charge estimation of lithium-ion battery based on extended state observer," vol. 131, p. 109994, 2020.

[5] J. Meng *et al.*, "An overview and comparison of online implementable SOC estimation methods for lithium-ion battery," vol. 54, no. 2, pp. 1583-1591, 2017.

[6] Y.-H. Chiang, W.-Y. Sean, and J.-C. J. J. o. P. S. Ke, "Online estimation of internal resistance and open-circuit voltage of lithium-ion batteries in electric vehicles," vol. 196, no. 8, pp. 3921-3932, 2011.

[7] I. Snihir, W. Rey, E. Verbitskiy, A. Belfadhel-Ayeb, and P. H. J. J. o. P. S. Notten, "Battery open-circuit voltage estimation by a method of statistical analysis," vol. 159, no. 2, pp. 1484-1487, 2006.

[8] X. Hu, S. Li, and H. J. J. o. P. S. Peng, "A comparative study of equivalent circuit models for Li-ion batteries," vol. 198, pp. 359-367, 2012.

[9] J. Zhu *et al.*, "Investigation of lithium-ion battery degradation mechanisms by combining differential voltage analysis and alternating current impedance," vol. 448, p. 227575, 2020.

[10] Z. Geng, T. Thiringer, and M. J. Lacey, "Intermittent current interruption method for commercial lithium-ion batteries aging characterization," *IEEE Transactions on Transportation Electrification,* vol. 8, no. 2, pp. 2985-2995, 2021.

[11] B. Aktekin *et al.*, "Understanding the capacity loss in LiNi0. 5Mn1. 5O4–Li4Ti5O12 lithium-ion cells at ambient and elevated temperatures," *The Journal of Physical Chemistry C,* vol. 122, no. 21, pp. 11234-11248, 2018.

[12] M. Kabir and D. E. J. I. J. o. E. R. Demirocak, "Degradation mechanisms in Li-ion batteries: a state-of-the-art review," vol. 41, no. 14, pp. 1963-1986, 2017.

[13] X. Han *et al.*, "A review on the key issues of the lithium ion battery degradation among the whole life cycle," vol. 1, p. 100005, 2019.

[14] W. Choi, H.-C. Shin, J. M. Kim, J.-Y. Choi, and W.-S. Yoon, "Modeling and applications of electrochemical impedance spectroscopy (EIS) for lithium-ion batteries," *Journal of Electrochemical Science and Technology,* vol. 11, no. 1, pp. 1-13, 2020.

[15] A. Guarino, W. Zamboni, and E. Monmasson, "A battery residual capacity indicator based on the battery internal resistance: An experimental study," in *2020 2nd IEEE International Conference on Industrial Electronics for Sustainable Energy Systems (IESES)*, 2020, vol. 1, pp. 15-20: IEEE.

[16] D. Anseán *et al.*, "Lithium-ion battery degradation indicators via incremental capacity analysis," *IEEE Transactions on Industry Applications,* vol. 55, no. 3, pp. 2992-3002, 2019.

[17] B. Jiang, C. Han, B. Li, Y. He, and Z. J. A. N. Lin, "In-situ crafting of ZnFe2O4 nanoparticles impregnated within continuous carbon network as advanced anode materials," vol. 10, no. 2, pp. 2728-2735, 2016.

[18] B. Jiang *et al.*, "Polymer-templated formation of polydopamine-coated SnO2 nanocrystals: anodes for cyclable lithium-ion batteries," vol. 56, no. 7, pp. 1869-1872, 2017.